

## Electrochemical Characterization of Intermediate-Temperature Solid Oxide Fuel Cells with PVD-Coated Electrolyte

To cite this article: Andrey Solovyev *et al* 2021 *ECS Trans.* **103** 105

View the [article online](#) for updates and enhancements.

## Electrochemical Characterization of Intermediate-Temperature Solid Oxide Fuel Cells with PVD-coated Electrolyte

A. Solovyev<sup>a</sup>, I. Burmistrov<sup>b</sup>, S. Rabotkin<sup>a</sup>, A. Shipilova<sup>a</sup>, D. Yalovenko<sup>b</sup>, V. Semenov<sup>a</sup>,  
and S. Bredikhin<sup>b</sup>

<sup>a</sup> Institute of High Current Electronics SB RAS, Tomsk, 634055, Russia

<sup>b</sup> Institute of Solid State Physics RAS, Chernogolovka, Moscow Region, 142432, Russia

Anode-supported solid oxide fuel cells with thin electrolyte show good electrochemical performance. In this work, 4- $\mu\text{m}$ -thick YSZ electrolyte with 2- $\mu\text{m}$ -thick GDC barrier layer is deposited onto the anode substrates by reactive magnetron sputtering. It is shown that high power density can be obtained for  $5 \times 5 \text{ cm}^2$  cells under planar stack conditions with stainless steel current collectors. Electrochemical investigations are performed in the temperature range of 600–800°C. High power density of 0.29, 0.83, 1.4  $\text{W cm}^{-2}$  is achieved at a voltage of 0.7 V and 600, 700, and 800°C, respectively.

### Introduction

Intermediate temperature solid oxide fuel cells (SOFCs) operating in the range of 600–800°C are of great interest today, since they widen the choice of materials, lower the system costs, and reduce the corrosion rate of the system components (1). The electrolyte thickness must be reduced in order to decrease the area specific resistance (ASR) of the fuel cell for its operating in this temperature range. For the formation of sub-micrometer thick electrolyte, physical vapor deposition (PVD), chemical vapor deposition or chemical solution deposition (sol-gel, spin-coating, dip-coating) are commonly used (2–6). Using the PVD methods, which include sputtering, it is easy to fabricate thin films with different chemical composition and high deposition rate. The possibility of obtaining dense gas-tight YSZ electrolyte films 3–5  $\mu\text{m}$  thick on  $13 \times 13$  and  $10 \times 10 \text{ cm}^2$  anodes by magnetron sputtering is demonstrated in several works (2, 7). Recent cost analysis shows that the high efficiency of cells with PVD-coated electrolyte reduces the production costs of SOFC stacks (8).

However, in order to get a high power density of the cell within the stack, it is not enough to reduce the electrolyte thickness. Stack performance depends not only on the cell resistance, but also on the resistance of various materials used in an SOFC stack and contact resistance between electrodes and interconnects, especially on the cathode side (9). The higher the contact resistance between various layers and the resistance of individual layers, the lower the stack output performance (10).

The ASR of small button cells is usually much less than that of industrial-sized planar anode-supported SOFC cells ( $10 \times 10 \text{ cm}^2$  or larger). This is not only due to the fact that current collector meshes made of noble metals are used to test button cells. With increasing cell area, it is more difficult to ensure the reliable contact between the cell and

the interconnect that leads to an increase in the contact resistance. For example, the power density of the proposed  $10 \times 5 \text{ cm}^2$  cell with magnetron sputtered yttria-stabilized zirconia (YSZ)/gadolinium-doped ceria (GDC) bilayer electrolyte and  $\text{La}_{0.6}\text{Sr}_{0.4}\text{Co}_{0.2}\text{Fe}_{0.8}\text{O}_3/\text{Gd}_{0.1}\text{Ce}_{0.9}\text{O}_{1.95}$  (LSCF/GDC) cathode is  $430 \text{ mW cm}^{-2}$  at 0.7 V and  $750^\circ\text{C}$  (11). This value is about 40% of that of the 2-cm diameter button cell ( $1025 \text{ mW cm}^{-2}$ ) with a similar structure and composition (12). At  $750^\circ\text{C}$ , the ASR of the former cell is  $0.54 \text{ Ohm cm}^2$ , while for the latter it is  $0.2 \text{ Ohm cm}^2$ .

Thus, the purpose of this work is to increase the performance of the large-area cell with the PVD-coated electrolyte under the conditions as close as possible to those existing in stacks. For this purpose, the interconnect design, structure and composition of the cathode active and cathode contact layers are improved.

## Experimental

### Cell Fabrication

YSZ and GDC electrolyte layers were deposited on the  $500 \mu\text{m}$  thick commercial anodes (Kceracell Co., Korea) with the size of  $5 \times 5 \text{ cm}^2$  using reactive dual magnetron sputtering. The process of electrolyte deposition was described in detail in (7). Substrates were mounted on a drum rotated during the deposition in order to provide the uniformity of the electrolyte thickness. The target-to-substrate distance was about 10 cm. Two metallic Zr–Y (86:14 at.%) and two metallic Ce–Gd (90:10 at.%) targets  $10 \times 30 \text{ cm}^2$  in size, with 99.5% purity were sputtered in Ar/O<sub>2</sub> atmosphere. The total chamber pressure was 0.67 Pa during sputtering. Before coating, the substrates were heated to  $450^\circ\text{C}$  by infrared heaters built into the drum with the substrates on it. The coating deposition was performed at 4 kW on the Zr–Y targets and at 3 kW on the Ce–Gd targets at a 45 kHz frequency. After the  $4 \mu\text{m}$  YSZ layer deposition, the  $2 \mu\text{m}$  thick GDC layer was deposited. The deposition rate was  $0.5$  and  $0.7 \mu\text{m h}^{-1}$  for YSZ and GDC layers, respectively.

The double-layer cathode consisting of LSCF/GDC and LSCF (Kceracell Co., Korea)  $4 \times 4 \text{ cm}^2$  layers was screen printed onto the electrolyte. It was fired to  $1100^\circ\text{C}$  for 2 hours to form sintered layers  $10 \mu\text{m}$  thick. To improve the contact between the double-layer LSCF/GDC|LSCF cathode and the cathode end plate, the LSC (Kceracell Co., Korea) cathode contact layer was deposited onto the cathode end plate before testing the fuel cell.

The microstructure of the obtained cells was studied on a Supra 50VP scanning electron microscope (Carl Zeiss, Germany).

### Cell Testing

Electrochemical performance of single cells was studied in the home-made fuel cell test rig. A cell was placed between end plates with gas channels. End plates were made of Crofer 22 APU stainless steel (ThyssenKrupp AG, Germany). Both cathode and anode end plates were coated with protective Ni coatings to effectively suppress the chromium diffusion to the interface with SOFC electrodes (13). The end plates had ribs and channels 1 and 2 mm wide, respectively (Figure 1). To improve the electrical contact and

reduce hydraulic resistance to the fuel gas flow, a nickel mesh (UMMC, Russia) was placed on the anode side. Compression gaskets cut from Thermiculite® 866 sheets (Flexitallic, UK) 0.7 mm thick, were used for sealing. The cell was heated and cooled at a rate of  $2\text{ }^{\circ}\text{C min}^{-1}$ . The control thermocouple was placed 3 mm below the anode end plate. Electrochemical cell measurements were performed in the temperature range of 600–800°C. Air was fed to the cathode as an oxidant at 1000 standard  $\text{cm}^3\text{ min}^{-1}$  (sccm), while the fuel was humidified (3%) hydrogen with the same flow rate. Following the anode reduction and upon receiving the stable open circuit voltage (OCV) signal, the I-V measurements were performed.

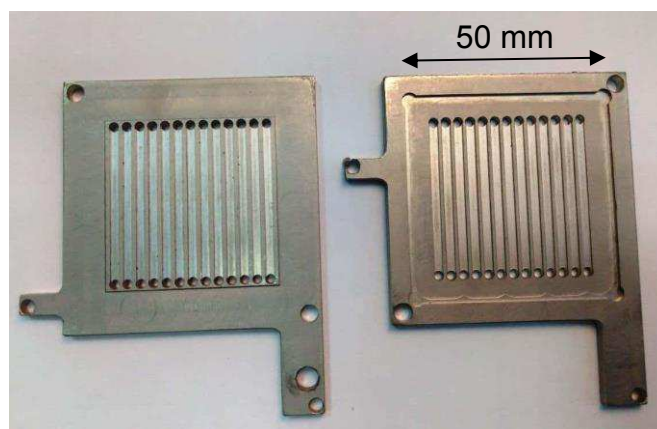


Figure 1. Photograph of cathode (left) and anode (right) end plates.

The I-V characteristics and impedance spectra were obtained by potentiostat-galvanostat and impedance meter Reference 3000 with the Reference 30K Booster (Gamry, Italy) attachment. Electrochemical impedance spectroscopy (EIS) was used to determine the impedance values for the unit cell. The impedance spectra were measured in the frequency range of 0.1 Hz–300 kHz under open circuit condition; the AC signal amplitude was 20 mV.

## Results and Discussion

### Cell Structure

In order to obtain a thin gas-tight electrolyte, the anode substrate should be provided with a functional layer as homogeneous and smooth as possible having small pores. Pores or inhomogeneities of the anode surface may cause pinholes in the thin electrolyte. Even small pinholes may cause a fuel crossover between the anode and cathode and unwanted chemical reactions on the cathode side of the fuel cell. Therefore, in this study, we use NiO/10ScCeSZ anodes with rather a dense and smooth 25  $\mu\text{m}$  thick anode functional layer (AFL) (Figure 2).

The SEM image of the fabricated cell cross-section is shown in Figure 3a. Thin YSZ and GDC electrolyte layers are uniformly and densely deposited on the anode substrate (Figure 3c). Electrolyte layers contain small closed pores of about 90 nm diameter. They are formed after the electrolyte annealing and recrystallization as a result of sintering of the film's columns to grains with the formation of closed porosity between the grains (14).

Small closed pores may decrease the ion conduction area. However, a significant decrease in the electrolyte conductivity resulting from closed pores, is unlikely because the pores and porosity are small. Sputtered GDC layer has a dense structure in contrast to layers obtained by sintering. The latter often have high porosity, which increases the ohmic resistance due to the low contact between YSZ and GDC and the diffusion of Sr to the YSZ|GDC interface with the formation of an insulating layer (15).

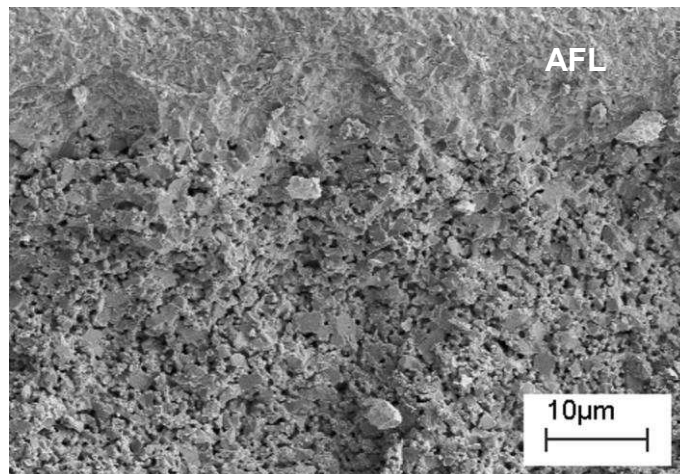


Figure 2. Cross-sectional SEM image of the of anode substrate microstructure.

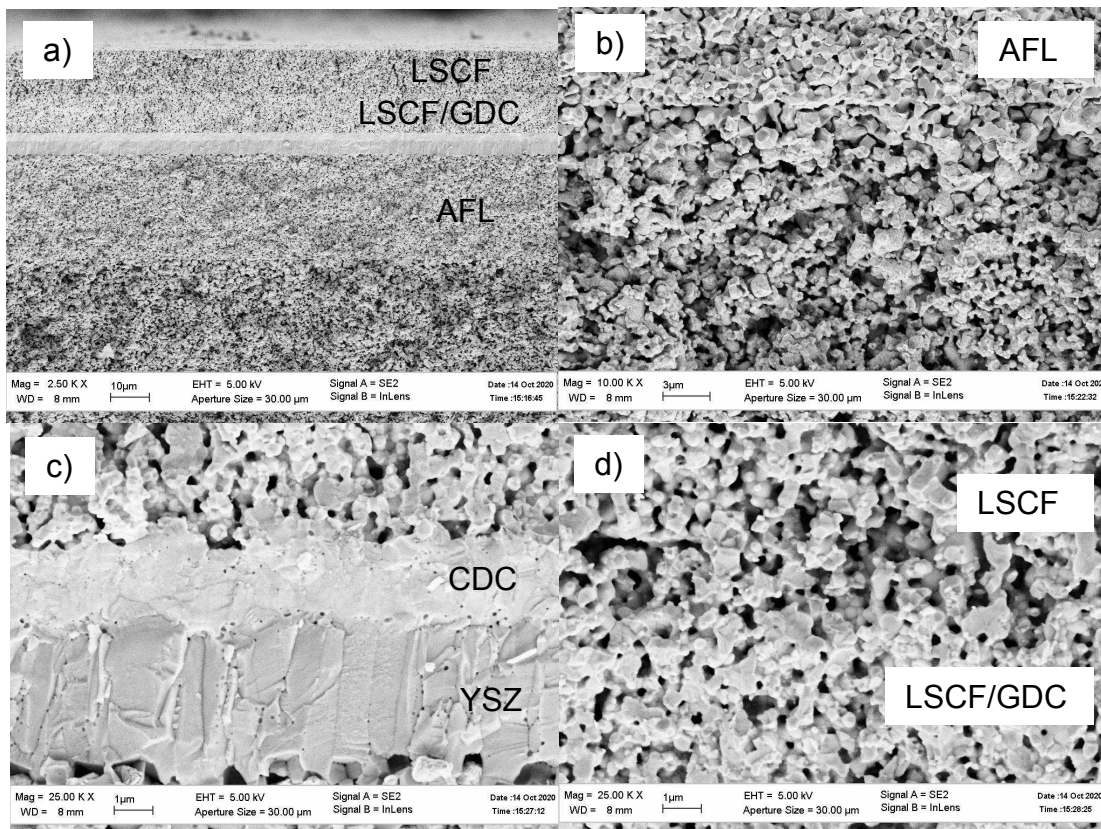


Figure 3. Cross-sectional SEM images of the cell (a), anode (b), YSZ|GDC electrolyte (c) and LSCF/GDC|LSCF cathode (d) microstructure after testing.

The size of the surface voids generated in a reducing environment in AFL, does not exceed 1  $\mu\text{m}$  (Figure 3b), which contributes to the mechanical stability of the thin electrolyte. The anode and cathode layers have a porous structure and adhere well to the electrolyte. This indicates that the thin electrolyte still retains its microstructure after high temperature measurements. Cathode LSCF/GDC and LSCF layers have the same thickness (10  $\mu\text{m}$ ), but the LSCF layer is more porous (Figure 3d).

### Electrochemical Performance Measurements

Figure 4a shows the resulting cell performance. The open circuit voltage (OCV) ranges between 1.08–1.1 V, depending on temperature, which is very close to the theoretical value. High power density of 0.29, 0.55, 0.83, 1.16 and 1.4  $\text{W cm}^{-2}$  is achieved at 0.7 V and 600, 650, 700, 750 and 800 $^{\circ}\text{C}$ , respectively. The area specific resistance obtained as the slope of the I-V curve is 0.725, 0.393, 0.276, 0.201 and 0.168  $\Omega\text{ cm}^2$  at 600, 650, 700, 750 and 800 $^{\circ}\text{C}$ , respectively. Thus, at 750 $^{\circ}\text{C}$ , the obtained 5  $\times$  5  $\text{cm}^2$  cell has even higher power density and lower ASR, than our button cell with the same PVD-coated YSZ|GDC electrolyte (12). The main differences between the obtained cell and the previously studied 10  $\times$  5  $\text{cm}^2$  (11) and button (12) cells include the anode substrate with a denser anode functional layer and the two-layer structure of the LSCF/GDC|LSCF cathode. Both of these factors affect the cell properties.

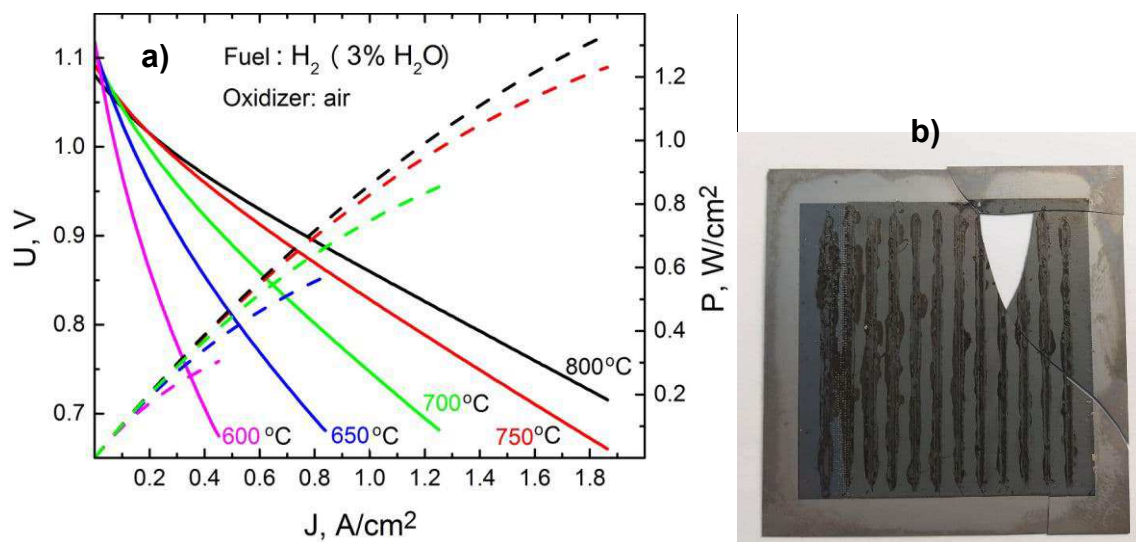


Figure 4. I–V–P curves of 5  $\times$  5  $\text{cm}^2$  cell with PVD-coated electrolyte (a) and the photograph of cell after testing (b).

Figure 4b shows the photograph of the cell after testing. The vertical black stripes represent residues of the LSC paste applied to the cathode end plate to reduce the contact resistance of the cathode/end plate interface. Using their dimensions, we can calculate the contact area between the two mating surfaces.

The resulting power density is slightly lower than that of the most advanced anode-supported SOFC from Forschungszentrum Jülich with a 1- $\mu\text{m}$  thick electrolyte (16). The obtained in Jülich power density serves as a main reference value for many SOFC developers. The power density of Ni-YSZ|YSZ|GDC|LSCF cells developed in Jülich with the active cathode size of 16  $\text{cm}^2$  is 1.89  $\text{W cm}^{-2}$  at 0.7 V and 800 $^{\circ}\text{C}$ . The power density

of our  $5 \times 5 \text{ cm}^2$  cells exceeds the values obtained in (17) for the Ni-YSZ|YSZ(1  $\mu\text{m}$ )|GDC(300 nm)|LSCF cells with the sputtered electrolyte. The power density of the latter is 150 and 250  $\text{mW cm}^{-2}$  at 0.7 V and 600 and 650°C, respectively (the active area of the single cell is 7.085  $\text{cm}^2$ ).

Figure 5 shows the electrochemical impedance spectra of the  $5 \times 5 \text{ cm}^2$  cell under the open circuit condition measured at different temperatures. The obtained impedance values of the cell are presented in Table I. The EIS results indicate that at all temperatures, the ohmic impedance is small part (about 11–15 %) of the total cell impedance representing the sum of ohmic and faradaic impedances ( $R_{\Omega} + R_F$ ). This means that the rate determining step of the cell operation in the cell with the thin PVD-coated electrolyte relates not to the conductivity of electrolyte, but the electrode reaction kinetics. The same is observed by Kang *et al.* (17) for cells with 1  $\mu\text{m}$  thick YSZ electrolyte.

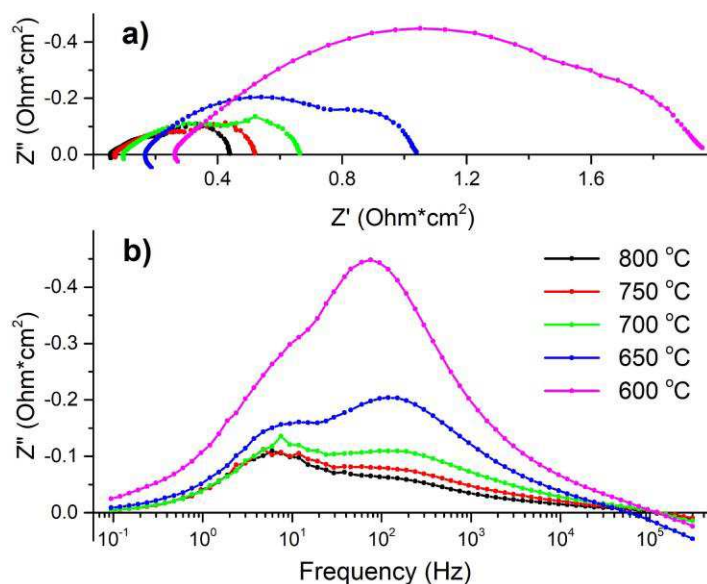


Figure 5. The impedance spectra at OCV for  $5 \times 5 \text{ cm}^2$  cell at 600–800°C: Nyquist (a) and Bode (b) plots.

**TABLE I.** Values of ohmic impedance  $R_{\Omega}$  and faradaic impedance  $R_F$  of  $5 \times 5 \text{ cm}^2$  cell.

Temperature (°C)	$R_{\Omega}$ (Ohm $\text{cm}^2$ )	$R_F$ (Ohm $\text{cm}^2$ )
800	0.055	0.385
750	0.070	0.450
700	0.095	0.570
650	0.165	0.875
600	0.260	1.700

Figure 5b shows that at low temperatures (600–650°C), the greatest contribution to the impedance is made by processes in the frequency range  $10^2$ – $10^3$  Hz. However, at higher temperatures (700–800°C), the processes in the frequency range  $10^0$ – $10^1$  Hz make the greatest contribution.

## Conclusions

In this work,  $5 \times 5 \text{ cm}^2$  anode-supported solid oxide fuel cells with thin YSZ|GDC electrolyte were fabricated. Microstructural analyses of the single-cell cross-section showed a uniform and dense thin-film electrolyte layer without pinholes or cracks. A Ni-YSZ|YSZ|GDC|LSCF/GDC|LSCF single cell with a 4  $\mu\text{m}$  thick YSZ layer and 2  $\mu\text{m}$  thick GDC layer showed the OCV of 1.08–1.1 V and the maximum power density of 0.29, 0.83, 1.4  $\text{W cm}^{-2}$  at 0.7 V and at 600, 700, and 800°C, respectively. The impedance spectroscopy demonstrated that the rate determining step for the developed SOFCs was the electrode kinetics.

### Acknowledgment

This work was financially supported by Grant No. 17-79-30071 from the Russian Science Foundation.

### References

1. D. J. L. Brett, A. Atkinson, N. P. Brandon, and S. J. Skinner, *Chem. Soc. Rev.*, **37**, 1568 (2008).
2. S. Sønderby, A. Aijaz, U. Helmersson, K. Sarakinos, and P. Eklund, *Surf. Coat. Technol.*, **240**, 1 (2014).
3. S. Heiroth, T. Lippert, A. Wokaun, M. Döbeli, J. L. M. Rupp, B. Scherrer, and L. J. Gauckler, *J. Eur. Ceram. Soc.*, **30**, 489 (2010).
4. N. V. Gelfond, O. F. Bobrenok, M. R. Predtechensky, N. B. Morozova, K. V. Zherikova, and I. K. Igumenov, *Inorg. Mater.*, **45**, 659 (2009).
5. C. C. Chen, M. M. Nasrallah, and H. U. Anderson, *Solid State Ion.*, **70/71**, 101 (1994).
6. C. Xia, S. Zha, W. Yang, R. Peng, D. Peng, and G. Meng, *Solid State Ion.*, **133**, 287 (2000).
7. A. Solovyev, I. Ionov, A. Lauk, S. Linnik, A. Shipilova, and E. Smolyanskiy, *J. Electrochem. En. Conv. Stor.*, **15**(4), 044501 (2018).
8. M. R. Weimar, L. A. Chick, D. W. Gotthold, and G. A. Whyatt, *Cost Study for Manufacturing of Solid Oxide Fuel Cell Power Systems*, DOE Report, United States, 2013. DOI: 10.2172/1126362
9. W. Wu, G. L. Wang, W. B. Guan, Y. F. Zhen, and W. G. Wang, *Fuel Cells*, **13**(5), 743 (2013).
10. V. A. C. Haanappel, I. C. Vinke, L. G. J. de Haart, and D. Stolten, in *Proceedings of the 18th World Hydrogen Energy Conference 2010*, D. Stolten and T. Grube, Editors, p. 255, Parallel Sessions Book 1: Fuel Cell Basics/Fuel Infrastructures, Essen: Forschungszentrum Jülich GmbH, Zentralbibliothek, Verlag (2010).
11. A. Solovyev, A. M. Lebedynskiy, A. V. Shipilova, I. V. Ionov, E. A. Smolyanskiy, A. L. Lauk, G. E. Remnev, and A. S. Maslov, *Fuel Cells*, **17**(3), 378 (2017).
12. A. A. Solovyev, A. V. Shipilova, I. V. Ionov, A. N. Kovalchuk, S. V. Rabotkin, and V. O. Oskirko, *J. Electron. Mat.*, **45**, 3921 (2016).
13. N. V. Demeneva, O. V. Kononenko, D. V. Matveev, V. V. Kharton, and S. I. Bredikhin, *Mater. Lett.*, **240**, 201 (2019).

14. H. Hidalgo, A. L. Thomann, T. Lecas, J. Vuillet, K. Wittman-Teneze, D. Damiani, E. Millon, and P. Brault, *Fuel Cells*, **13**, 279 (2013).
15. Z. G. Lu, X. D. Zhou, J. Templeton, and J. W. Stevenson, *J. Electrochem. Soc.*, **157**, B964 (2010).
16. F. Han, R. Mücke, T. Van Gestel, A. Leonide, N. H. Menzler, H. P. Buchkremer, and D. Stöver, *J. Power Sources*, **218**, 157 (2012).
17. S. Kang, J. Lee, G. Y. Cho, Y. Kim, S. Lee, S. W. Cha, and J. Bae, *Int. J. Hydrog. Energy*, **45**(58), 33980 (2020).